Hindawi
Mathematical Problems in Engineering
Volume 2017, Article ID 9576950, 11 pages
https://doi.org/10.1155/2017/9576950

Research Article

Dynamic Magnetic Resonance Imaging Reconstruction Based on Nonconvex Low-Rank Model

Lixia Chen,[1,2] Bin Yang,[1] and Xuewen Wang[2,3]

[1]*School of Mathematics and Computing Science and Guangxi Colleges and Universities Key Laboratory of Data Analysis and Computation, Guilin University of Electronic Technology, Guilin, Guangxi 541004, China*
[2]*Guangxi Experiment Center of Information Science, Guilin, Guangxi 541004, China*
[3]*School of Computer Science and Information Security, Guilin University of Electronic Technology, Guilin, Guangxi 541004, China*

Correspondence should be addressed to Xuewen Wang; befine@aliyun.com

Received 13 July 2017; Revised 12 October 2017; Accepted 5 November 2017; Published 19 December 2017

Academic Editor: Francesco Soldovieri

Copyright © 2017 Lixia Chen et al. This is an open access article distributed under the Creative Commons Attribution License, which permits unrestricted use, distribution, and reproduction in any medium, provided the original work is properly cited.

The quality of dynamic magnetic resonance imaging reconstruction has heavy impact on clinical diagnosis. In this paper, we propose a new reconstructive algorithm based on the $L + S$ model. In the algorithm, the l_1 norm is substituted by the l_p norm to approximate the l_0 norm; thus the accuracy of the solution is improved. We apply an alternate iteration method to solve the resulting problem of the proposed method. Experiments on nine data sets show that the proposed algorithm can effectively reconstruct dynamic magnetic resonance images.

1. Introduction

Image reconstruction is widely applied in the medical field, and most clinical diagnoses depend on computer hardware equipment; thus the improvement on image reconstruction algorithm has great significance. At present, among all kinds of detection methods, magnetic resonance imaging (MRI) and computed tomography (CT) are the most common and important ways for clinical diagnosis. When checking organs by MR, the final image is affected in varying degrees by artifacts, which results in degrading in quality and affects the diagnoses. Therefore, reconstruction algorithms with high quality and fast calculation have become one of the research focuses in this field.

In recent years, in order to ensure image quality and to speed up the pace of reconstruction, there emerge many improved methods, such as multicoil parallel imaging [1], keyhole imaging technology [2, 3], unfold method [4], and k-t SENSE [5]. After the theory of compressed sensing (CS) [6, 7] was proposed, many scholars applied it to the dynamic MR reconstruction [5, 8, 9]. These methods process the original data by downsampling method instead of traditional full-sampling and reduce the computing time.

Since the development of robust principal component analysis (RPCA) theory [10], breakthroughs have emerged in the field of MR image reconstruction. This theory suggests that images with spatiotemporal correlation can be decomposed into low-rank (LR) matrices and sparse matrices. Many researchers introduced this theory to reconstruct dynamic MR images to achieve better results. In [11], a method was proposed based on accelerated diffusion weighted sequences for image reconstruction by the $L + S$ decomposition. In [12], 3D cardiac MRI was reconstructed by combining $L + S$ decomposition with prior knowledge. In [13], a new $L + S$ model was proposed, which decomposed a series of dynamic MR images with temporal and spatial correlation into LR matrices and sparse matrices. As a result, the dynamic MRI could be divided into the foreground and background to help diagnosis. In order to reconstruct dynamic MR images with better quality, based on the traditional $L + S$ model, a rank-1 and sparse model was proposed in [14].

Recently, a lot of researchers focused on the problem of l_0 norm approximation [15–17]. In particular, in [15], Candés et al. pointed out that a nonconvex problem can be transformed into a convex optimization problem using the l_1 norm instead of l_0 norm. However, the l_1 norm and l_0 norm

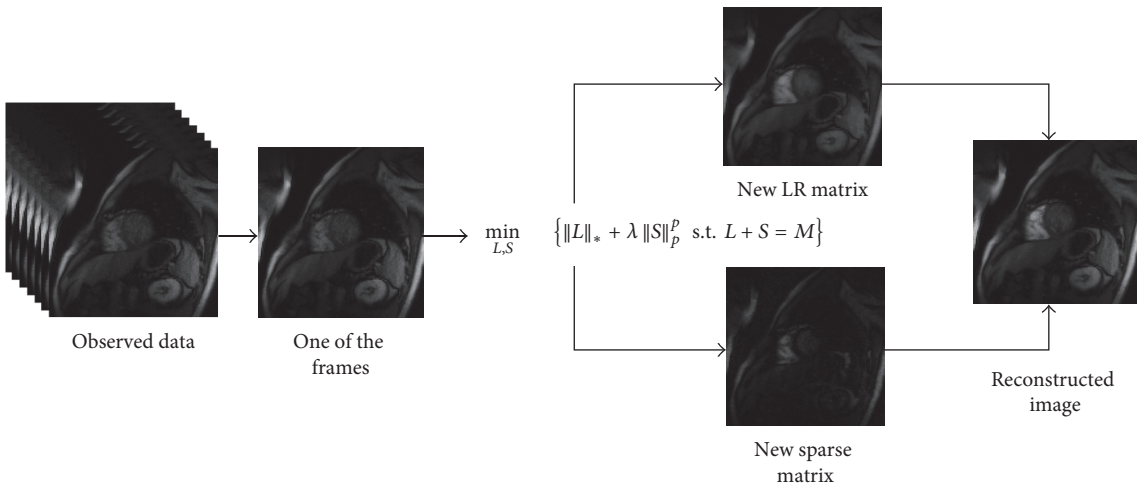

Figure 1: Framework of the proposed dynamic MRI reconstruction.

are still different in numerical values. For example, Sun et al. suggested that if the nuclear norm of the matrix is regarded as a l_1 norm and the rank of the matrix is regarded as a l_0 norm, the error between them can not be ignored in [18]. The algorithm in [19] achieved good approaching effect by introducing a nonconvex regularization which was like a l_p norm. In [20], Quach et al. proposed a nonconvex online RPCA model which enhanced the sparsity by minimization of the l_p norm and achieved good results in many fields, such as face modeling and online background removal.

Inspired by the above discussion, combining RPCA theory with a nonconvex idea, we propose a new MR image reconstruction model. The contributions of this paper are as follows: (1) in order to better approximate l_0 norm, we introduce a nonconvex regularization using the l_p norm instead of the l_1 norm. (2) The alternating direction method of multipliers (ADMM) is used to solve the nonconvex problem. In addition, we point out that the solution is convergent. The framework of this proposed method is shown in Figure 1.

The rest of this paper is organized as follows: in Section 2, a review of the $L + S$ model is presented. In Section 3, we firstly introduce the proposed model and then provide the detailed implementation of the proposed model. Finally, we illustrate the convergence of the proposed algorithm. In Section 4, in order to verify the effectiveness of our algorithm, comparisons between our method and the state-of-the-art algorithms are provided. In Section 5, we conclude our works.

2. Related Works

According to the theory of RPCA [10], we focus on the model

$$\min_{L,S} \quad \{\text{rank}\,(L) + \lambda \|S\|_0 \ \text{ s.t. } L + S = M\}, \tag{1}$$

where M is the observed data, L and S are the LR and the sparse matrix, respectively, $M, L,$ and $S \in R^{m\times n}$, and λ denotes the regularization parameter.

Since (1) is a nonconvex optimization problem, the effective solution of the problem is not easy to obtain [21]. According to the theory of RPCA, Otazo et al. [13] used the nuclear norm of L and the l_1 norm of S instead of the rank of L and the l_0 norm of S in (1), respectively, and proposed a convex optimization problem ($L + S$ model):

$$\min_{L,S} \quad \{\|L\|_* + \lambda \|S\|_1 \ \text{ s.t. } L + S = M\}, \tag{2}$$

where $\|\cdot\|_*$ is the nuclear norm. $\|\cdot\|_1$ denotes l_1 norm, which is the sum of absolute values of the elements in matrix S.

Let the data of an image correspond to the data of the k-t space by introducing an encoding operator E. And assume T to be the sparse transformation of S; that is, the dynamic component S can be expressed by the known sparse basis T. So the minimization problem (2) can be written as

$$\min_{L,S} \quad \{\|L\|_* + \lambda \|TS\|_1 \ \text{ s.t. } E\,(L + S) = d\}. \tag{3}$$

Singular Value Thresholding (SVT) algorithm [15] is introduced to solve the minimization problem (3).

3. The Proposed Model

3.1. Modeling. Although the above methods have good theoretical guarantee and have made major breakthroughs in dynamic MR image reconstruction, l_1 norm can not well approximate l_0 norm [15, 16, 20]. In addition, authors of [20, 22] pointed out that, among common nonconvex functions, such as q-norm [23], SCAD [24], log [15], MCP [25], ETP [26], and Geman [27], q-norm is the best approximation to l_0 norm. Inspired by this, we propose a new model as follows:

$$\min_{L,S} \quad \left\{\|L\|_* + \lambda \|S\|_p^p \ \text{ s.t. } E\,(L + S) = d\right\}, \tag{4}$$

where L is a LR matrix, S is a sparse matrix, and $\|\cdot\|_p$ denotes l_p norm. d is an undersampled observed data in the k-t space and $(L+S) \in R^{n\times n}$ denotes the ideal reconstructed MR image, where $n \times n$ denotes the size of the image. E is an encoding operator, which makes the data of an image correspond to the data of the k-t space.

Defining the p norm as $(\cdot) = |\cdot|_p$, the minimization problem (4) can be written as

$$\min_{L,S} \left\{ \|L\|_* + \lambda \sum_{i,j=1}^{n\times n} f\left(s_{i,j}\right) \text{ s.t. } E(L+S) = d \right\}, \quad (5)$$

where $s_{i,j}$ denotes the elements of S located in ith row and jth column, $i = 1, 2, \ldots, n$, and $j = 1, 2, \ldots, n$. And assume that the nonconvex function $f : R \to R^+$ is continuous and monotonically increasing on $[0, \infty)$.

Combining the properties of supergradient for nonsmooth points with Taylor expansion [20], the second term of (5) can be approximated as

$$\sum_{i,j=1}^{n\times n} f\left(s_{i,j}\right) = \sum_{i,j=1}^{n\times n} f\left(s_{i,j}^{(k)}\right) + \left\langle \nabla f\left(s_{i,j}^{(k)}\right), s_{i,j} - s_{i,j}^{(k)} \right\rangle, \quad (6)$$

where k is the number of iterations.

Therefore, the new model can be further expressed as

$$\min_{L,S} \left\{ \|L\|_* + \lambda \left(\sum_{i,j=1}^{n\times n} f\left(s_{i,j}^{(k)}\right) + \left\langle \nabla f\left(s_{i,j}^{(k)}\right), s_{i,j} - s_{i,j}^{(k)} \right\rangle \right) \text{ s.t. } E(L+S) = d \right\}. \quad (7)$$

3.2. Solving the Model. By introducing a Lagrangian multiplier, (7) turns to be an unconstrained minimization problem as

$$(L, S, Y, \mu) = \min_{L,S,Y,\mu} \left\{ \lambda_L \|L\|_* + \lambda_S \left(\sum_{i,j=1}^{n\times n} f\left(s_{i,j}^{(k)}\right) + \left\langle \nabla f\left(s_{i,j}^{(k)}\right), s_{i,j} - s_{i,j}^{(k)} \right\rangle \right) + \left\langle Y, E^H(E(L+S) - d) \right\rangle + \frac{\mu}{2} \left\| E^H(E(L+S) - d) \right\|_F^2 \right\}, \quad (8)$$

where λ_L and λ_S are regularization parameters which balance the nuclear norm and the l_p norm. Y denotes a Lagrangian multiplier, and μ is a penalty parameter. In order to solve (8), we divide it into two subproblems as

$$L^{(k+1)} = \arg\min_L \left\{ \lambda_L \|L\|_* + \frac{\mu^{(k)}}{2} \left\| E^{\mathrm{H}}\left(E\left(S^{(k)} + L\right) - d\right) - \frac{Y^{(k)}}{\mu^{(k)}} \right\|_F^2 \right\}, \quad (9)$$

$$S^{(k+1)} = \arg\min_S \left\{ \lambda_S \left(\sum_{i,j=1}^{n\times n} f\left(s_{i,j}^{(k)}\right) + \left\langle \nabla f\left(s_{i,j}^{(k)}\right), s_{i,j} - s_{i,j}^{(k)} \right\rangle \right) + \frac{\mu^{(k)}}{2} \left\| E^H\left(E\left(L^{(k+1)} + S\right) - d\right) - \frac{Y^{(k)}}{\mu^{(k)}} \right\|_F^2 \right\}. \quad (10)$$

When $S^{(k)}$ is obtained, we solve (9) by the Singular Value Thresholding (SVT) algorithm [15], and the solution is

$$L^{(k+1)} = \mathrm{SVT}_\tau\left(E^H\left(E\left(S^{(k)}\right) - d\right) - \frac{Y^{(k)}}{\mu^{(k)}} \right), \quad (11)$$

where $\mathrm{SVT}_\tau(X) = U[\mathrm{diag}(\Sigma - \tau I)_+]V^T$, $(x)_+ = \max(x, 0)$, and τ is a positive constant.

When $L^{(k+1)}$ is computed, the minimization problem (10) is equivalent to

$$S^{(k+1)} = \arg\min_S \left\{ \lambda_S \left(\sum_{i,j=1}^{n\times n} v_{i,j}^{(k)} \left| s_{i,j} \right| \right) + \frac{\mu^{(k)}}{2} \left\| E^H\left(E\left(L^{(k+1)} + S\right) - d\right) - \frac{Y^{(k)}}{\mu^{(k)}} \right\|_F^2 \right\}, \quad (12)$$

where

$$v_{i,j}^{(k)} = \nabla f\left(s_{i,j}^{(k)}\right) = p\left(\left|s_{i,j}\right| + \varepsilon\right)^{p-1} \quad (13)$$

and ε is a small positive real number to avoid the case that the gradient is 0. The minimization problem (12) is solved by the soft-thresholding algorithm [20, 28] as follows:

(1) **Input:** Observed k-t data d, encoding operator E, regularization parameter λ_L, λ_S;
(2) **Initialize:** $L^{(0)} = M^{(0)} = E^H d$, $S^{(0)} = 0$, $k = 0$, $\mu^{(0)} > 0$, $v_{ij}^{(0)} = 1$, $Y^{(0)} = E^H d / \sigma(E^H d)$;
(3) **Solving (4) via an alternate iteration method**
While not convergence do
  Update $L^{(k+1)}$ by (11);
  Update $S^{(k+1)}$ and $v_{ij}^{(k+1)}$ by (13) and (14), respectively;
  Update $M^{(k+1)}$ by (15);
  Update $Y^{(k+1)}$ and $\mu^{(k+1)}$ by (16) and (17), respectively;
  $k = k + 1$;
End while
(4) **Output:** $\widehat{L} = L^{(k+1)}$, $\widehat{S} = S^{(k+1)}$, $\widehat{M} = \widehat{L} + \widehat{S}$.

Algorithm 1: Dynamic MRI reconstruction algorithm based on nonconvex low-rank model.

$$S^{(k+1)} = S_{\lambda_S / \mu^{(k)} \times v^{(k)}} \left(E^H \left(E \left(L^{(k+1)} \right) - d \right) - \frac{Y^{(k)}}{\mu^{(k)}} \right), \quad (14)$$

where $S_\eta(z_i)$ is a soft-thresholding operator which is defined as $S_\eta(z_i) = \max(|z_i| - \eta, 0)(z_i / |z_i|)$ and $\eta = \lambda_S / \mu^{(k)} \times v^{(k)}$ is a threshold.

In the iteration process, after $L^{(k+1)}$ and $S^{(k+1)}$ are computed, we update $M^{(k+1)}$ by

$$\begin{aligned} M^{(k+1)} &= L^{(k+1)} + S^{(k+1)} \\ &\quad - E^H \left(E \left(L^{(k+1)} + S^{(k+1)} \right) - d \right), \end{aligned} \quad (15)$$

where $E^H(E(L^{(k+1)} + S^{(k+1)}) - d)$ represents artifacts, which is subtracted from the updating $L^{(k+1)} + S^{(k+1)}$ as a residual, resulting in a clearer image [22].

Finally, the parameters Y and μ are updated as follows:

$$Y^{(k+1)} = Y^{(k)} + \mu^{(k)} E^H \left(E \left(L^{(k+1)} + S^{(k+1)} \right) - d \right), \quad (16)$$

$$\mu^{(k+1)} = \rho \mu^{(k)}, \quad (17)$$

where $\rho > 1$. The complete process of this algorithm is shown in Algorithm 1.

According to [20], the above solving process is convergent.

Theorem 1 (see [20]). *Let $\{L^{(k)}, S^{(k)}\}$ be the sequences generated by Algorithm 1, and $F(L^{(k)}, S^{(k)})$ is monotonically decreasing; that is, $F(L^{(k)}, S^{(k)}) - F(L^{(k+1)}, S^{(k+1)}) \geq 0$. Then the sequences $\{L^{(k)}, S^{(k)}\}$ are bounded and have at least one gathering point.*

4. Numerical Experimental Comparisons and Analysis

In order to evaluate the performance of the proposed model, we compare our algorithm with the k-t SENSE [5], XD-GRASP [9], and the LplusS [13]. All experiments are run on a PC with Intel Core i5-4690 processor, 8 GB of memory, Win 7 64-bit operating system, and MATLAB 2014a. The quality of the reconstructed image is evaluated by the root mean square error (RMSE), which is defined as

$$\text{RMSE} = \frac{\|d - E(L + S)\|_F}{\|d\|_F}, \quad (18)$$

where d is the observation data and L and S are the LR matrix and sparse matrix for the reconstructed image, respectively. The smaller the RMSE is, the better the MR image is reconstructed.

The iteration stop indicator for all algorithms of this paper is linked to the relative error (Err), which is defined as

$$\text{Err} = \frac{\left\| L^{(k+1)} + S^{(k+1)} - \left(L^{(k)} + S^{(k)} \right) \right\|_F}{\left\| L^{(k)} + S^{(k)} \right\|_F}. \quad (19)$$

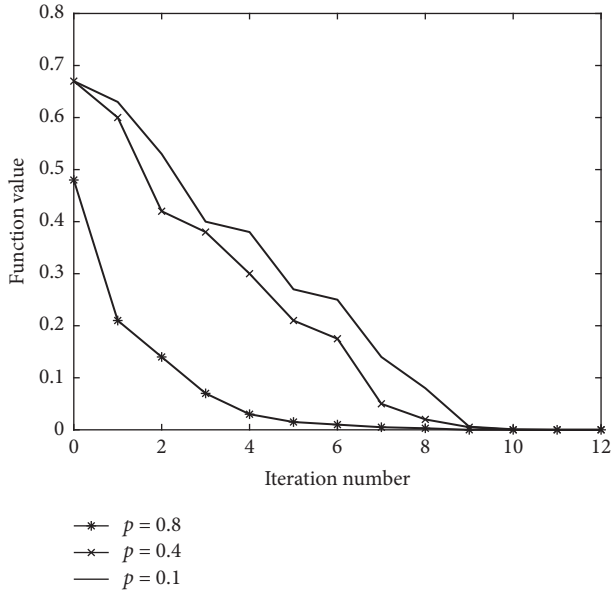

Figure 2: The relationship between the function values and the parameter p.

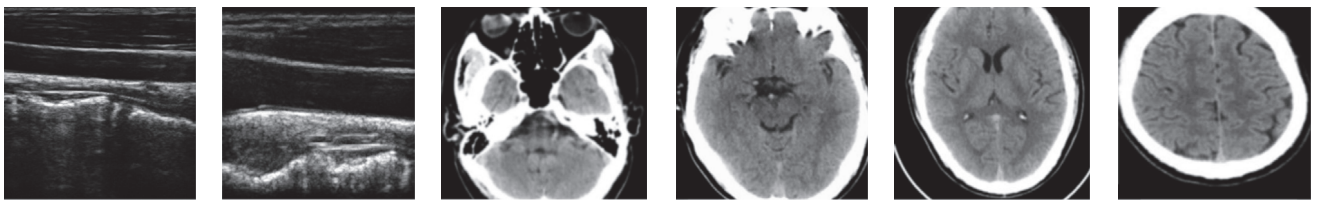

(a) (b) (c) (d) (e) (f)

Figure 3: The 5th frame of each data set. (a)–(f) are named as image 1 to image 6.

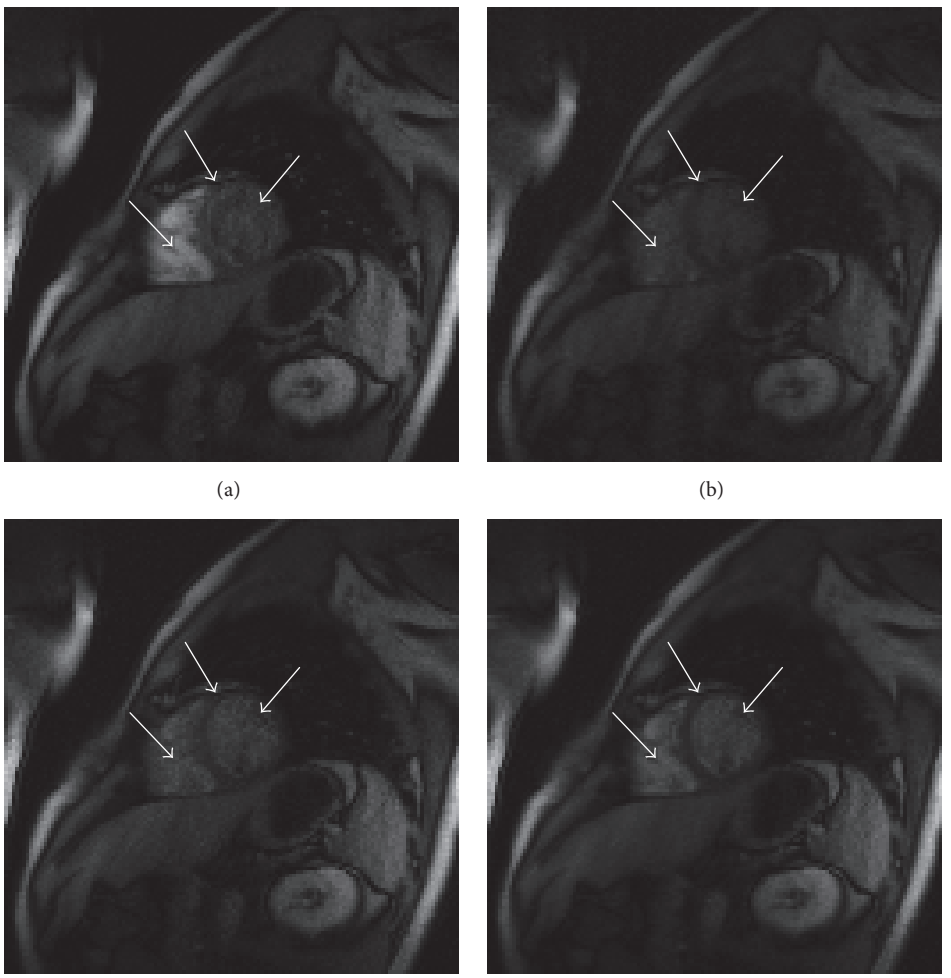

(a) (b)

(c) (d)

Figure 4: Reconstruction comparisons on the first frame of dynamic cardiac perfusion. (a) *k-t* SENSE, (b) XD-GRASP, (c) LplusS, and (d) our algorithm.

The iteration stops when the Err reduction of the consecutive iterations is less than a predefined threshold.

4.1. Experimental Data and the Selection of Parameters. There are nine sets of test data in this paper, three of them are open-data which come from [13], and the others are from a research institution, which are shown in Figure 3. The gray value of all the images ranges from 0 to 255. The values of τ, ρ, and ε are the choices of the best reconstruction after repeated tests. For all data in this paper, we set $\tau = 0.0025$, $\varepsilon = 0.0001$, and $\rho = 1.2$.

One of the three sets of open-data is the dynamic cardiac perfusion data, which consists of 40 images with size 128×128. The second is the dynamic cardiac cine data which is

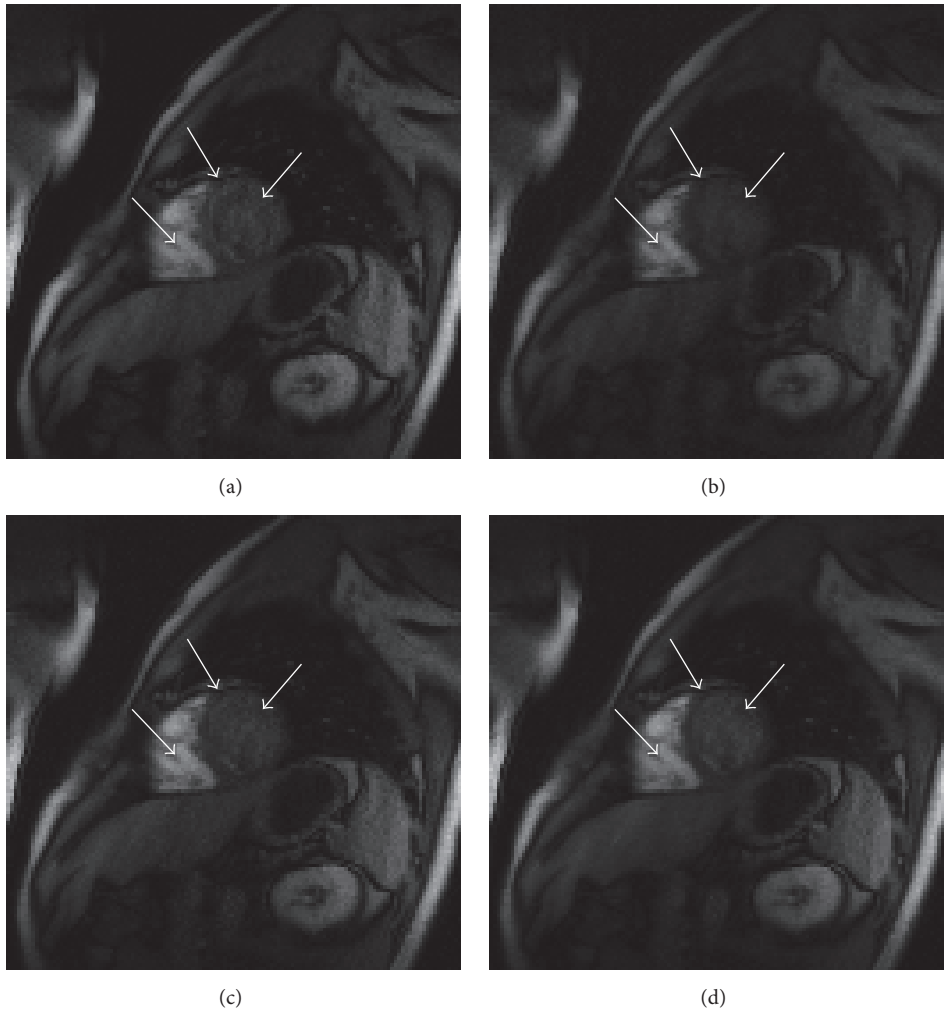

(a) (b) (c) (d)

Figure 5: Reconstruction comparisons on the 3rd frame of dynamic cardiac perfusion. (a) *k-t* SENSE, (b) XD-GRASP, (c) LplusS, and (d) our algorithm.

made up of 25 images with size 256×256. And the third is dynamic abdominal data which is composed of 28 images with size 384×384. The parameter combinations (λ_L, λ_S) for data set one to three are $(0.01, 0.025)$, $(0.015, 0.017)$, and $(0.025, 0.0125)$, respectively. When the Err is less than 2.5×10^{-3}, we stop the iteration for the dynamic cardiac perfusion and cardiac cine images. And, for dynamic abdomen images, the iteration stopping threshold is 3.5×10^{-2}. The other six data sets from the research institution are all composed of 15 images with size 384×384 for each set. For image 1, we set $\lambda_L = 0.0135$ and $\lambda_S = 0.014$, for image 2 we set $\lambda_L = 0.0137$ and $\lambda_S = 0.018$, and, for the remaining four images, we let $\lambda_L = 0.013$ and $\lambda_S = 0.02$, and the Err is set as 3.7×10^{-2}.

For p norm $(0 < p < 1)$, the choice of p heavily influences the convergence rate. Figure 2 shows the convergence rate with $p = 0.1$, 0.4, and 0.8. The greater p results in the faster convergence rate. A large number of experiments also prove that the smaller p leads to the smaller Err and the more precise solution. Through repeated trials, we set $p = 0.2$ in all experiments for our algorithm.

4.2. Comparisons and Analysis. In this section, we compare our method with the *k-t* SENSE, XD-GRASP, and LplusS algorithm in subjective and objective aspects. Figures 4–9 present the visual comparisons, and the differences between the reconstructions by four algorithms are depicted with white arrows. The comparisons on RMSE, Err, and time consumption are listed in Tables 1 and 2, where the boldfaced numbers are the best results of all.

Figures 4 and 5 are the reconstructed comparisons of the first frame and the fifth frame of dynamic cardiac perfusion, respectively. Figure 4(d) is the best reconstructed image of Figure 4. In Figures 4(a) and 4(b), the edge contours of organs at the top right corner are blurred, and the details pointed out by the white arrows are not clear. Only Figure 4(c) is comparable to Figure 4(d), but, at the places of the bottom

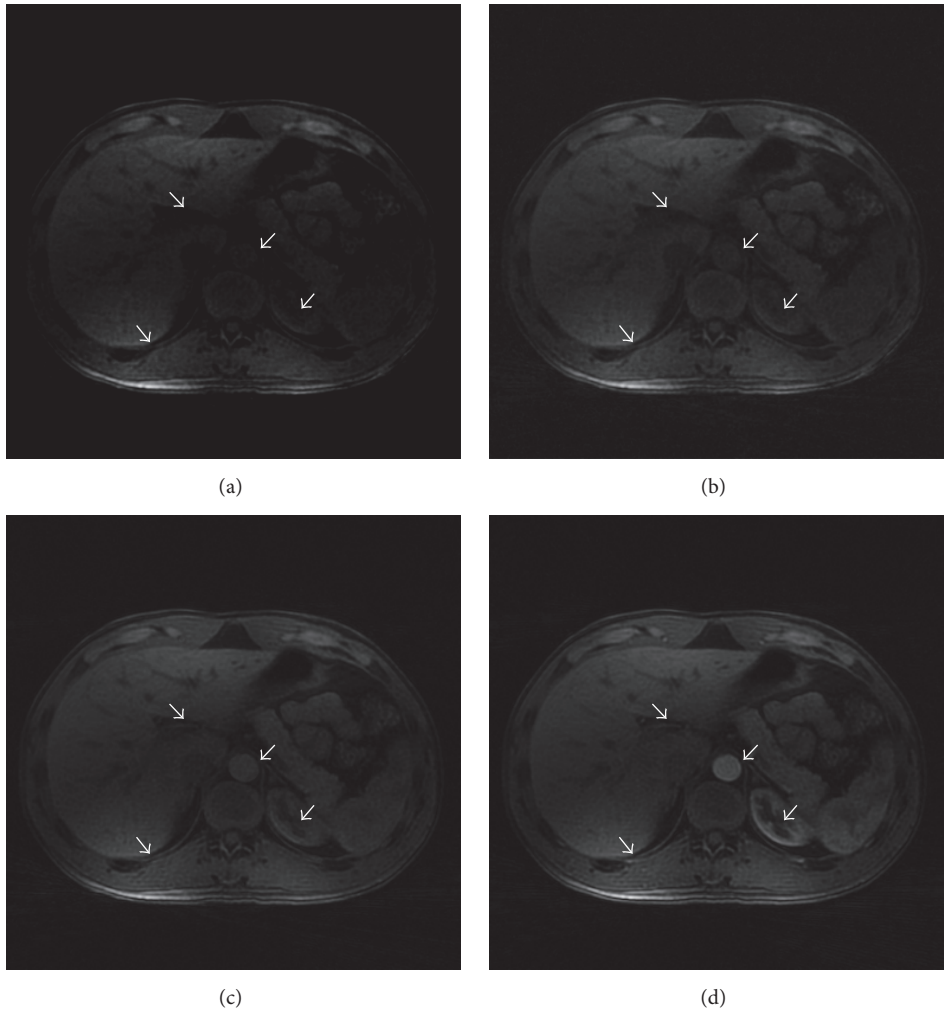

(a) (b) (c) (d)

Figure 6: Reconstruction comparisons on the 2nd frame of dynamic abdomen. (a) k-t SENSE, (b) XD-GRASP, (c) LplusS, and (d) our algorithm.

left and upper right arrows, local details contain more noise, which causes the characteristics of organ unobtrusiveness and is not conducive to disease diagnosis. Figure 5(d) is obviously clearer than Figures 5(a) and 5(b) and superior to Figure 5(c) in the place that the white arrows indicate.

Figures 6 and 7 represent the reconstructions about the dynamic abdomen image with the second frame and the fifth frame, respectively. By comparing, the proposed algorithm is better than the other three algorithms in brightness and resolution.

Figure 8 shows the reconstructed images of the 20th frame of the cardiac cine. The reconstruction effects of all four algorithms have no obvious visual differences, but, through careful observation on the enlarged regions to which the white arrows point, the proposed algorithm performs better.

Figure 9 shows the reconstructed effects of images 1, 2, 4, and 6, respectively. In images 1 and 2, we find that the features of our algorithm are the most obvious among four compared methods, especially in the regions where the white arrows point. In images 4 and 6, the outline and details of the organ of the proposed algorithm are clearer than those of the other reference algorithms, and the result is brighter.

Tables 1 and 2 list the numerical results of the four algorithms. The proposed algorithm ranks the first on the Err and RMSE among the four comparison methods, which denotes that the reconstruction quality is the best. Of all experiments, the time consumption of our algorithm is the second best except for cardiac cine in Table 1, on which the proposed algorithm ranks the first.

5. Conclusions

In this paper, we propose a nonconvex model for reconstructing high-quality dynamic MR images. In the new model, based on the RPCA theory, the l_1 norm is substituted by the l_p norm to approximate the l_0 norm; thus the accuracy of the solution is improved. An alternate iteration method is applied to solve the proposed model. Experimental results show that the proposed algorithm has advantages in terms of visual effect, RSME, and Err over three reference algorithms.

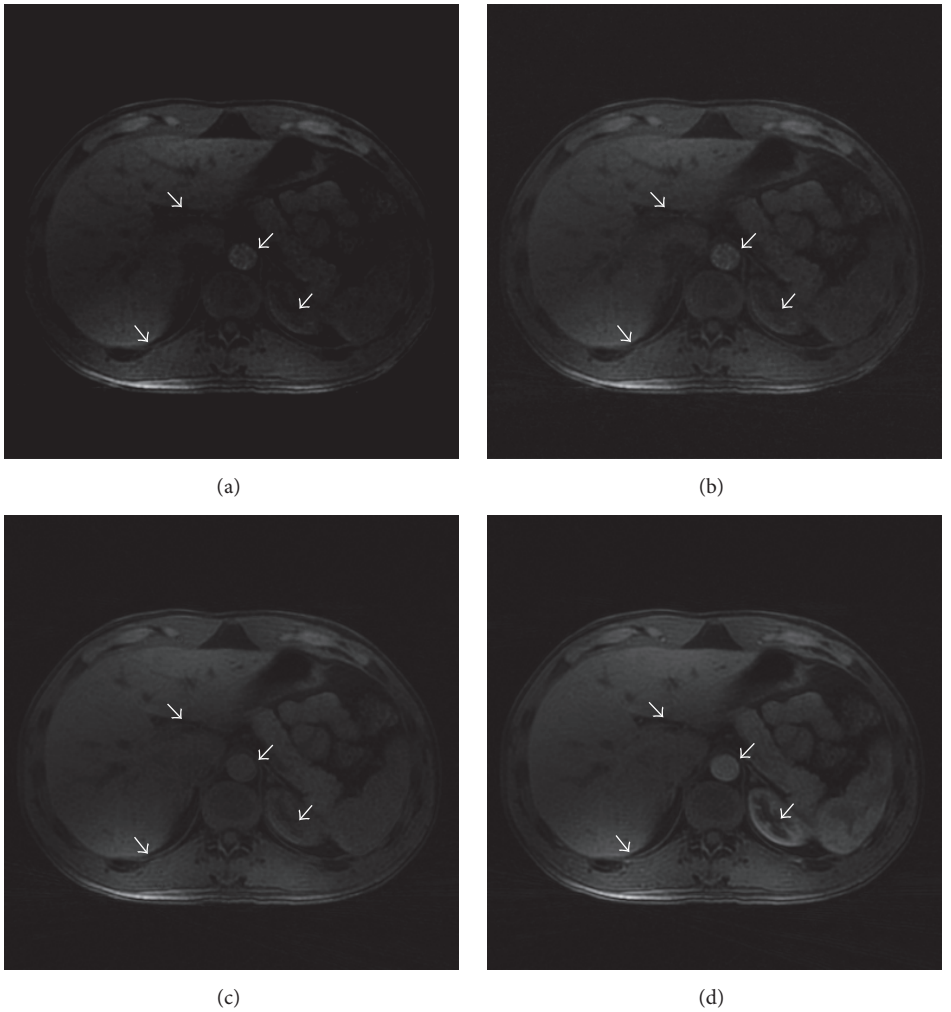

(a) (b) (c) (d)

Figure 7: Reconstruction comparisons on the 5th frame of dynamic abdomen. (a) *k-t* SENSE, (b) XD-GRASP, (c) LplusS, and (d) our algorithm.

Table 1: Comparison on object indexes.

Image		*k-t* SENSE	XD-GRASP	LplusS	Ours
Cardiac perfusion	Err	2.50×10^{-3}	2.50×10^{-3}	2.42×10^{-3}	$\mathbf{2.32 \times 10^{-3}}$
	RMSE	0.8124	0.8013	0.8009	**0.7880**
	Time (s)	220.4	202.4	**83.9**	84.2
Abdomen images	Err	3.50×10^{-2}	3.23×10^{-2}	2.56×10^{-2}	$\mathbf{2.53 \times 10^{-2}}$
	RMSE	12.4521	11.7607	9.2530	**9.2465**
	Time (s)	336.2	310.3	**293.1**	293.8
Cardiac cine	Err	2.48×10^{-3}	2.50×10^{-3}	2.47×10^{-3}	$\mathbf{2.40 \times 10^{-3}}$
	RMSE	0.5233	0.5147	0.5063	**0.5059**
	Time (s)	156.0	159.0	141.7	**108.1**

But, in terms of time consumption, the proposed algorithm is slightly inferior to LplusS, which requires further improvement.

Conflicts of Interest

The authors declare that they have no conflicts of interest.

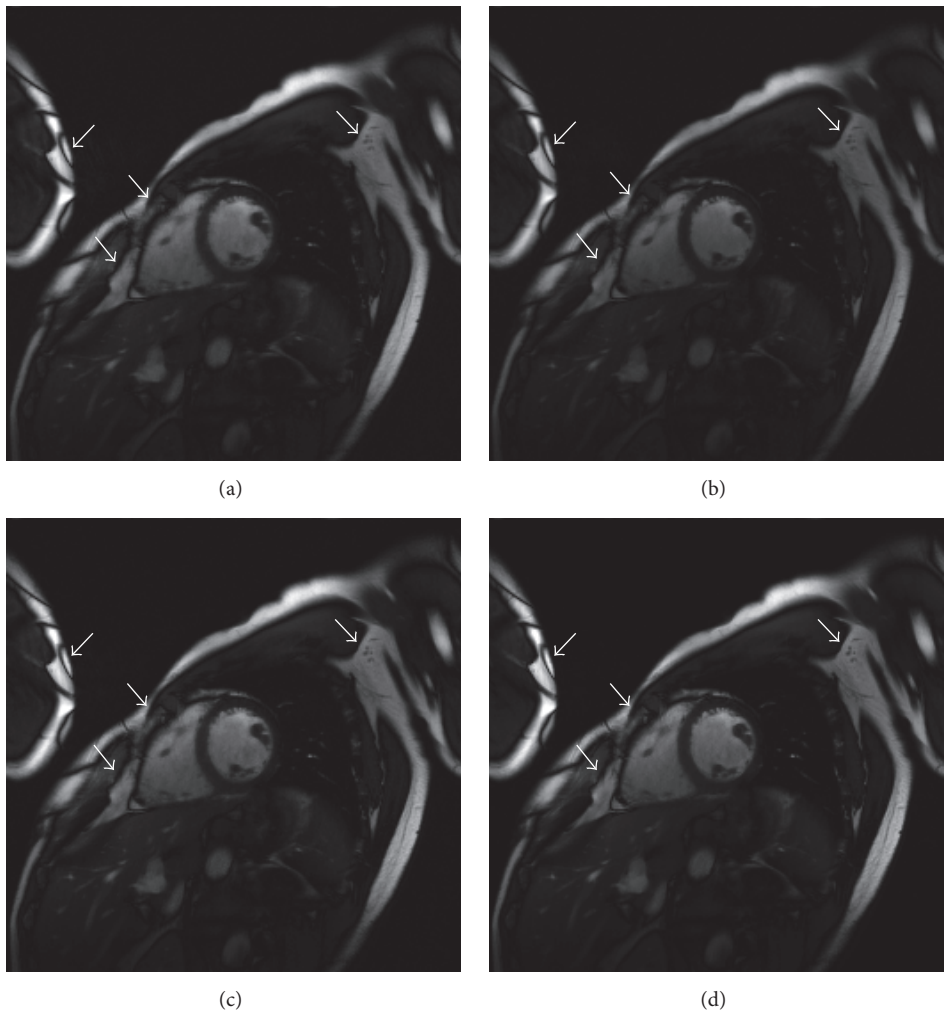

(a) (b) (c) (d)

Figure 8: Reconstruction comparisons on the 20th frame of dynamic cardiac cine. (a) *k-t* SENSE, (b) XD-GRASP, (c) LplusS, and (d) our algorithm.

Table 2: Comparison on object indexes.

Image		*k-t* SENSE	XD-GRASP	LplusS	Ours
Image 1	Err	3.70×10^{-2}	3.25×10^{-2}	3.11×10^{-2}	$\mathbf{2.93 \times 10^{-2}}$
	RMSE	9.7235	9.3785	8.2500	**7.9798**
	Time (s)	202.0	185.3	**162.3**	171.6
Image 2	Err	3.62×10^{-2}	3.35×10^{-2}	3.23×10^{-2}	$\mathbf{3.20 \times 10^{-2}}$
	RMSE	12.7820	10.2324	9.4725	**9.2849**
	Time (s)	196.1	188.4	**153.2**	185.2
Image 3	Err	3.43×10^{-2}	3.07×10^{-2}	2.95×10^{-2}	$\mathbf{2.73 \times 10^{-2}}$
	RMSE	5.2474	3.2596	2.9487	**2.6503**
	Time (s)	153.0	147.8	**107.9**	110.8
Image 4	Err	3.70×10^{-2}	3.54×10^{-2}	3.03×10^{-2}	$\mathbf{2.88 \times 10^{-2}}$
	RMSE	12.2844	11.5627	9.0751	**8.8329**
	Time (s)	214.3	193.1	**159.4**	169.0
Image 5	Err	3.58×10^{-2}	3.45×10^{-2}	2.97×10^{-2}	$\mathbf{2.84 \times 10^{-2}}$
	RMSE	10.7704	9.8403	8.7709	**7.8322**
	Time (s)	189.7	163.2	**125.9**	144.3
Image 6	Err	3.50×10^{-2}	3.37×10^{-2}	3.05×10^{-2}	$\mathbf{2.94 \times 10^{-2}}$
	RMSE	8.5527	8.2764	7.3008	**6.8425**
	Time (s)	157.5	140.6	**118.3**	135.7

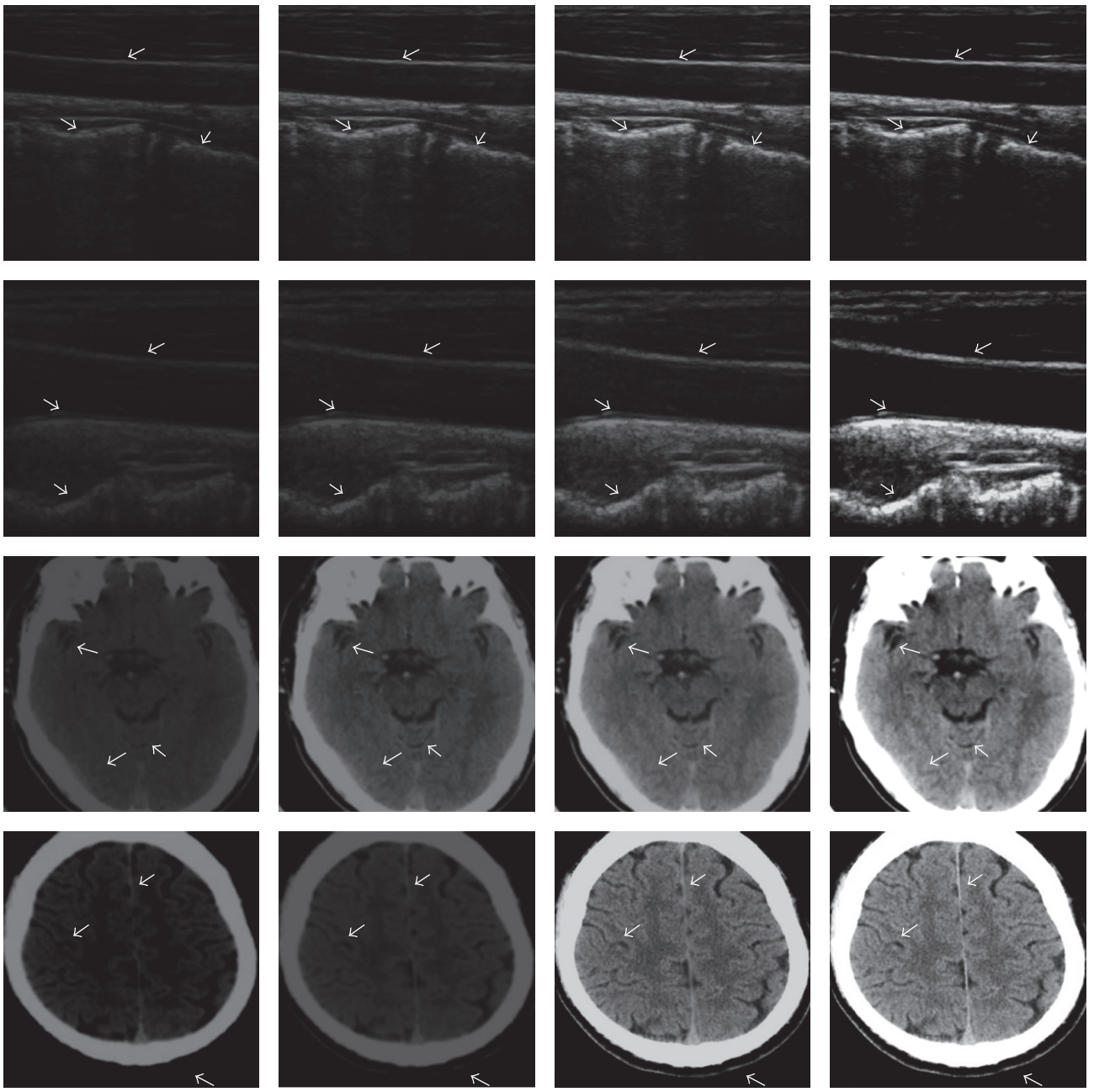

Figure 9: Reconstruction comparisons on four images. From top to bottom are images 1, 2, 4, and 6, respectively. From left to right are *k*-*t* SENSE, XD-GRASP, LplusS, and our algorithm, respectively.

Acknowledgments

This project is partially supported by the National Natural Science Foundation of China (61362021, 61661017, 61272216, and 61572147), Guangxi Natural Science Foundation (2013GXNSFDA019030, 2014GXNSFAA118003, and 2016GXNSFAA380043), Guangxi Colleges and Universities Key Laboratory of Intelligent Processing of Computer Images and Graphics (GIIP201408, GIIP201503), Guangxi Colleges and Universities Key Laboratory of Data Analysis and Computation (LDAC201704), Basic Research Capacity Promotion Project for Youth and Middle-Aged Teachers in Colleges and Universities of Guangxi (ky2016YB162), and Project of Education Innovation Project of Guilin University of Electronic Science and Technology (2017YJCX84).

References

[1] M. Blaimer, M. Choli, P. M. Jakob, M. A. Griswold, and F. A. Breuer, "Multiband phase-constrained parallel MRI," *Magnetic Resonance in Medicine*, vol. 69, no. 4, pp. 974–980, 2013.

[2] R. A. Jones, O. Haraldseth, T. B. Müller, P. A. Rinck, and A. N. Øksendal, "K-space substitution: A novel dynamic imaging technique," *Magnetic Resonance in Medicine*, vol. 29, no. 6, pp. 830–834, 1993.

[3] E. Subashi, E. J. Moding, G. P. Cofer et al., "A comparison of radial keyhole strategies for high spatial and temporal resolution 4D contrast-enhanced MRI in small animal tumor models," *Medical Physics*, vol. 40, no. 2, Article ID 022304, pp. 1–10, 2013.

[4] S.-H. Kim and C.-K. Kang, "A dual K-space UNFOLD method for 3D functional brain imaging: a preliminary study," *Magnetic Resonance Imaging*, vol. 34, no. 2, pp. 120–126, 2016.

[5] J. Tsao, P. Boesiger, and K. P. Pruessmann, "k-t BLAST and k-t SENSE: dynamic MRI with high frame rate exploiting spatiotemporal correlations," *Magnetic Resonance in Medicine*, vol. 50, no. 5, pp. 1031–1042, 2003.

[6] E. J. Candes and M. B. Wakin, "An introduction to compressive sampling: a sensing/sampling paradigm that goes against the common knowledge in data acquisition," *IEEE Signal Processing Magazine*, vol. 25, no. 2, pp. 21–30, 2008.

[7] D. Gangopadhyay, E. G. Allstot, A. M. R. Dixon, K. Natarajan, S. Gupta, and D. J. Allstot, "Compressed sensing analog front-end for bio-sensor applications," *IEEE Journal of Solid-State Circuits*, vol. 49, no. 2, pp. 426–438, 2014.

[8] R. Jia and H. Du, "Motion compensated dynamic MRI reconstruction exploiting sparsity and low rank structure," in *Proceedings of the 13th IEEE International Conference on Signal Processing (ICSP '16)*, pp. 19–22, November 2016.

[9] L. Feng, R. Grimm, K. T. O. Block et al., "Golden-angle radial sparse parallel MRI: combination of compressed sensing, parallel imaging, and golden-angle radial sampling for fast and flexible dynamic volumetric MRI," *Magnetic Resonance in Medicine*, vol. 72, no. 3, pp. 707–717, 2014.

[10] S. Javed, S. K. Jung, A. Mahmood, and T. Bouwmans, "Motion-Aware Graph Regularized RPCA for background modeling of complex scenes," in *Proceedings of the 2016 23rd International Conference on Pattern Recognition (ICPR '16)*, pp. 120–125, December 2016.

[11] H. Gao, S. Rapacchi, D. Wang et al., "Compressed sensing using prior rank, intensity and sparsity model(prism): applications in cardiac cine mri," in *Proceedings of the 20th Annual Meeting of ISMRM*, vol. 15, pp. 3736–3745, Melbourne, Australia, 2012.

[12] D. Zonoobi, S. Faghigh roohi, and A. A. Kassim, "Low-rank and sparse matrix decomposition with a-priori knowledge for dynamic 3D MRI reconstruction," in *Proceedings of the International Conference on Bioimaging*, pp. 82–88, Lisbon, Portugal, January 2015.

[13] R. Otazo, E. J. Candès, and D. K. Sodickson, "Low-rank plus sparse matrix decomposition for accelerated dynamic MRI with separation of background and dynamic components," *Magnetic Resonance in Medicine*, vol. 73, no. 3, pp. 1125–1136, 2015.

[14] X. Xiu and L. Kong, "Rank-one and transformed sparse decomposition for dynamic cardiac MRI," *BioMed Research International*, vol. 2015, Article ID 169317, 7 pages, 2015.

[15] E. J. Candés, M. B. Wakin, and S. P. Boyd, "Enhancing sparsity by reweighted l1 minimization," *Journal of Fourier Analysis and Applications*, vol. 14, no. 5-6, pp. 877–905, 2008.

[16] Sa. C. De, K. Olukotun, and R. Christopher, "Global convergence of stochastic gradient descent for some non-convex matrix problems," in *Proceesings of the International Conference on 32nd International Conference on Machine Learning*, pp. 2332–2341, Lille, France, July 2015.

[17] X. Chen, D. Ge, Z. Wang, and Y. Ye, "Complexity of unconstrained l2-lp minimization," *Mathematical Programming*, vol. 143, no. 1-2, pp. 371–383, 2014.

[18] Q. Sun, S. Xiang, and J. Ye, "Robust principal component analysis via capped norms," in *Proceedings of the ACM SIGKDD International Conference on Knowledge Discovery and Data Mining*, pp. 311–319, Chicago, IL, USA, August 2013.

[19] Y. Xie, Y. Qu, D. Tao, W. Wu, Q. Yuan, and W. Zhang, "Hyperspectral image restoration via iteratively regularized weighted schatten p-norm minimization," *IEEE Transactions on Geoscience and Remote Sensing*, vol. 54, no. 8, pp. 4642–4659, 2016.

[20] K. G. Quach, C. N. Duong, K. Luu, and T. D. Bui, "Non-convex online robust PCA: enhance sparsity via ℓp-norm minimization," *Computer Vision and Image Understanding*, vol. 158, pp. 126–140, 2017.

[21] S. Boyd and L. Vandenberghe, *Convex Optimization*, Cambridge University Press, 2004.

[22] F. Xu, J. Han, Y. Wang et al., "Dynamic magnetic resonance imaging via nonconvex low-rank matrix approximation," *IEEE Access*, vol. 5, pp. 1958–1966, 2017.

[23] B. D. Rao and K. Kreutz-Delgado, "An affine scaling methodology for best basis selection," *IEEE Transactions on Signal Processing*, vol. 47, no. 1, pp. 187–200, 1999.

[24] J. Fan and R. Li, "Variable selection via nonconcave penalized likelihood and its oracle properties," *Journal of the American Statistical Association*, vol. 96, no. 456, pp. 1348–1360, 2001.

[25] C.-H. Zhang, "Nearly unbiased variable selection under minimax concave penalty," *The Annals of Statistics*, vol. 38, no. 2, pp. 894–942, 2010.

[26] C. Gao, N. Wang, Q. Yu, and Z. Zhang, "A feasible nonconvex relaxation approach to feature selection," in *Proceedings of the AAAI Conference on Artificial Intelligence*, pp. 356–361, 2011.

[27] Z. Kang, C. Peng, and Q. Cheng, "Robust PCA via nonconvex rank approximation," in *Proceedings of the 15th IEEE International Conference on Data Mining (ICDM '15)*, pp. 211–220, November 2015.

[28] W. Dong, G. Shi, X. Li, Y. Ma, and F. Huang, "Compressive sensing via nonlocal low-rank regularization," *IEEE Transactions on Image Processing*, vol. 23, no. 8, pp. 3618–3632, 2014.

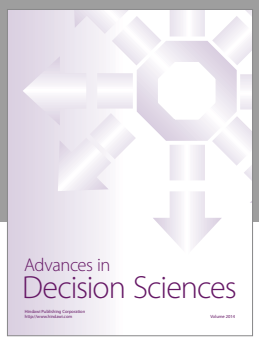

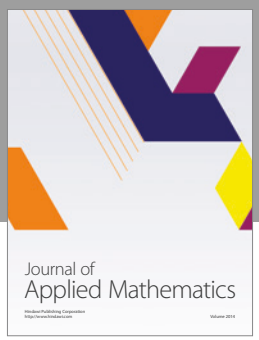

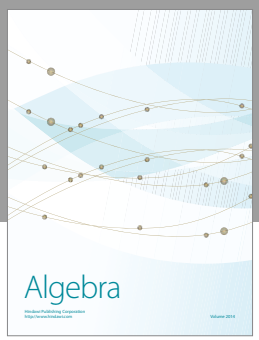

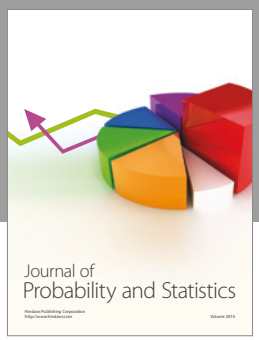

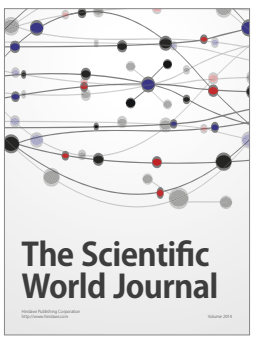

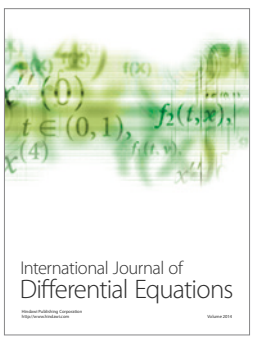

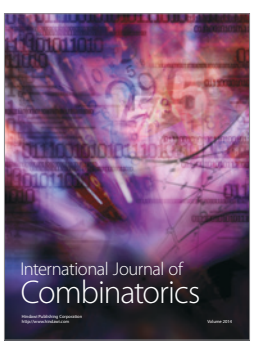

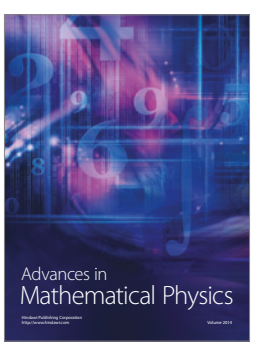

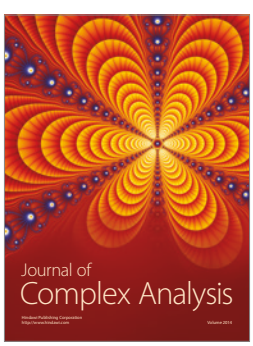

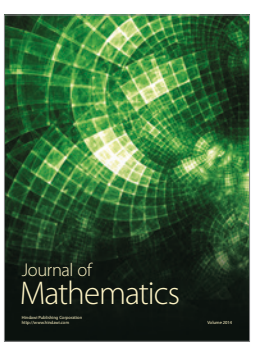

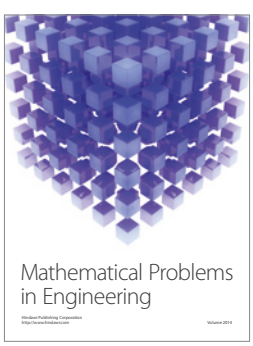

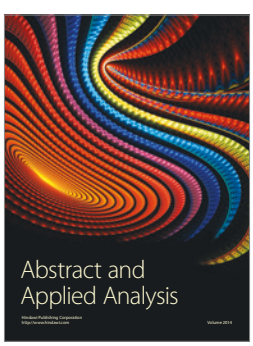

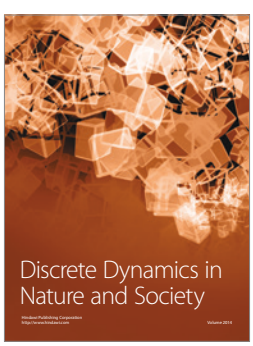

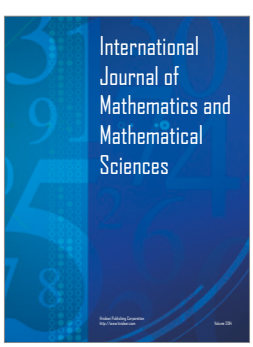

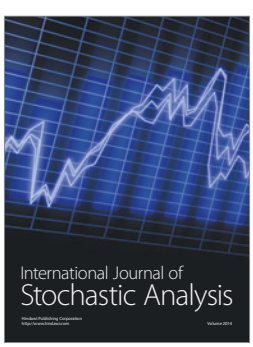

Hindawi

Submit your manuscripts at
https://www.hindawi.com